Earthquakes in quasistatic models of fractures in elastic media: formalism and numerical techniques

1997 J. Phys. A: Math. Gen. 30 2297

(http://iopscience.iop.org/0305-4470/30/7/012)

J. Phys. A: Math. Gen. **30** (1997) 2297–2315. Printed in the UK PII: S0305-4470(97)74783-8

Earthquakes in quasistatic models of fractures in elastic media: formalism and numerical techniques

Kan Chen†, Ravi Bhagavatula‡ and C Jayaprakash§

† Department of Computational Science, National University of Singapore, Singapore 0511
‡ Department of Physics and Astronomy, University of Pittsburgh, Pittsburgh, PA 15260, USA
§ Department of Physics, The Ohio State University, Columbus, OH 43210, USA

Received 20 May 1996, in final form 10 October 1996

Abstract. We present the details of a formalism for a self-consistent description of multiple ruptures in an elastic medium and numerical techniques for studying quasistatic processes of fractures. We apply this formalism and investigate a double-couple model of a seismic zone with an embedded pre-existing fault. Results for both spatial and temporal features of earthquakes and power laws in statistical distributions are presented.

1. Introduction

There has been considerable interest in studying fracture processes in heterogeneous solids [1]. Discrete models based on a network of bonds or plaquettes have been typically used to study fractures in heterogeneous materials where the existence of many microcracks and inhomogeneities in local breakdown thresholds play a significant role. Such models are important not only for elucidating the microscopic aspects of the strength of composite or disordered materials, but are also crucial for understanding earthquakes, which involve large-scale fractures caused by the slow relative motion of tectonic plates [2]. There are different approaches to studying this problem, ranging from simple lattice models with central forces (block spring) to those that include angular stiffness all the way to formal finite element techniques. There is an extensive literature on this subject [1]. The study of lattices near the percolation threshold has also generated considerable interest. A plaquette model of elastic media in the presence of local ruptures has been constructed recently by Xu *et al* [3]. They showed that the effects of local ruptures can be represented correctly by a local double-couple force distribution; this representation allows efficient simulation of the fracture process. The plaquette model also leads to a more direct connection with the continuum description [4], as the stress and strain tensors are defined locally on individual plaquettes.

In this paper we describe the details of a new numerical technique for studying fractures in a large class of quasistatic models. In addition, we will also present an efficient method for evaluating the lattice Green functions used in calculating the stress redistribution due to local ruptures. The formalism is general and can also be used to study a variety of other breakdown problems, such as random fuse network problems [6–8] and dielectric breakdown problems [9]. The other method that can be fruitfully employed is the conjugate gradient method [5]. We note that, however, our method is especially effective for the cases in which the number of ruptures is small in comparison with the number of plaquettes.

0305-4470/97/072297+19$19.50

We illustrate the application of our numerical scheme by studying a double-couple model of a seismic zone with an embedded pre-existing fault. We provide numerical evidence that suggests that the power-law behaviour of the model remains the same as in our earlier dipole model [10, 11]. On a more technical note, the original discretization scheme of [3] exhibits some non-physical features, as will be explained in detail later, such as the problem of sublattice decoupling and an ambiguity in the direction of fractures at the level of a unit plaquette. This paper presents a refined discretization scheme that avoids these problems that is of interest in the general context of discretizing continuum elastic problems.

The rest of the paper is organized as follows. In section 2 we describe our refined discretization scheme and review the general self-consistent procedure for calculating the stress redistribution due to multiple ruptures using lattice Green functions [10]. In section 3 we present new numerical techniques for simulating the quasistatic process of fractures. Section 4 begins with a brief summary of earlier studies of earthquake models and then details the application of our numerical scheme to a double-couple model of the seismic zone with an embedded pre-existing fault. This double-couple model in which both the force- and torque-balance conditions following a rupture are incorporated (thus reflecting the full tensorial nature of elasticity theory) generalizes the dipole version of the model introduced earlier by us [11]. Numerical results on the spatial and temporal features of the model will be presented. As in our previous studies, we consider two-dimensional systems and include only fractures along the direction of the external shear for greater computational feasibility. Some technical details are relegated to two appendices; an efficient method for calculating Green functions is presented in appendix A and an iterative scheme for inverting matrices is reviewed in appendix B.

2. Formalism and discretization scheme

In this section we will discuss our formalism for handling multiple ruptures in a heterogeneous elastic medium. While these considerations apply equally well to modelling the fracture of disordered, brittle materials under external stress we present the ideas in the context of earthquakes. Consider an elastic region (the seismic zone) with possible macroscopic inhomogeneities (for example, a pre-existing fault); the elastic medium is assigned random thresholds for local fractures. External loading (tectonic forces) results in the build-up of stress leading to a sequence of ruptures. The quasistatic version of the general problem that must be solved consists of two parts.

The first part corresponds to static equilibrium within linear elasticity which is described by the force-balance condition on the stress tensor, σ_{ij}, that applies wherever there are no ruptures:

$$\frac{\partial \sigma_{ij}}{\partial x_i} = 0. \tag{2.1}$$

Recall the definition of the (continuum) strain tensor

$$u_{ij}(\boldsymbol{r}) = \frac{1}{2}\left(\frac{\partial u_j(\boldsymbol{r})}{\partial x_i} + \frac{\partial u_i(\boldsymbol{r})}{\partial x_j}\right) \tag{2.2}$$

where $u_i(\boldsymbol{r})$ is the ith component of the displacement vector at $\boldsymbol{r}$. In the absence of ruptures, when all deformations are elastic, the stress tensor is related to the strain tensor through the generalized Hooke's law:

$$\sigma_{ij}(\boldsymbol{r}) = K u_{ll}(\boldsymbol{r})\delta_{ij} + 2\mu(u_{ij}(\boldsymbol{r}) - \tfrac{1}{3}\delta_{ij}u_{ll}(\boldsymbol{r})) \tag{2.3}$$

where K and μ are the bulk and shear moduli respectively and summation over repeated indices is implied.

The second part involves dealing with local ruptures and their effect on the stress in the medium. In order to handle this problem we discretize the system and consider a square lattice. Let us consider the effect of a local rupture, say, a shear fracture in the $\hat{e}_x$ direction at a plaquette $\boldsymbol{r}_0$. We have tacitly assumed that the length scale of the rupture is set by the lattice spacing determined by the discretization procedure, thereby adopting a macroscopic description of the fracture process. After the break we must decide on an appropriate boundary condition at the fracture (see the discussion in section 4); given the boundary condition, for example, that the shear stress on the fractured surface is reduced to a fraction of the original stress, there is a force imbalance resulting in a stress redistribution. The calculation we must do is to find a self-consistent solution for the stresses in the presence of multiple ruptures that satisfies the specified boundary conditions at the ruptures (and fault segments) and the static, elastic, equilibrium conditions elsewhere. In this section we discuss the technical aspects of the discretization scheme on a two-dimensional lattice, the various problems associated with naive schemes and one way of overcoming these; we also present a method for evaluating the necessary Green functions efficiently. We point out that we have reduced the problem to a two-dimensional one by imposing a plane stress condition, i.e. all the stresses act in the xy plane. In this case it is easy to verify that the bulk modulus, K, in equation (2.3) is an effective modulus that is related to the three-dimensional moduli.

The discretization scheme in [3] for elastic systems is defined by introducing the discretized derivatives, D_i, along the ith direction of a square lattice as follows; for any function $g(\boldsymbol{r})$ we define,

$$D_x g(\boldsymbol{r}) \equiv \tfrac{1}{2}[g(\boldsymbol{r}+\boldsymbol{b}) + g(\boldsymbol{r}+\boldsymbol{d}) - g(\boldsymbol{r}-\boldsymbol{b}) - g(\boldsymbol{r}-\boldsymbol{d})] \tag{2.4}$$

and

$$D_y g(\boldsymbol{r}) \equiv \tfrac{1}{2}[g(\boldsymbol{r}+\boldsymbol{b}) + g(\boldsymbol{r}-\boldsymbol{d}) - g(\boldsymbol{r}+\boldsymbol{d}) - g(\boldsymbol{r}-\boldsymbol{b})] \tag{2.5}$$

where we have defined $\boldsymbol{d} = (\hat{e}_x - \hat{e}_y)/2$ and $\boldsymbol{b} = (\hat{e}_x + \hat{e}_y)/2$ in terms of the unit vectors $\hat{e}_x$ and $\hat{e}_y$ along the coordinate axes. We imagine that the displacement vectors $\{\boldsymbol{u}(\boldsymbol{r})\}$ are defined at the centres of the squares or plaquettes; then the stress tensors $\{\sigma_{ij}(\boldsymbol{r})\}$ are defined at the corners of the squares. Using this scheme, Xu *et al* [3] have shown that the local ruptures can be represented along double couples with fictitious forces residing at the corners of the fractured plaquettes. The effect of local ruptures on the stress and displacement distributions of the system can be represented by Green functions. Let $u_i'(\boldsymbol{r})$ denote the additional displacement induced by the rupture. The additional stress caused by the rupture σ_{ij}' can be divided into a part σ_{ij}^{el} that is related to u_i' via the generalized Hooke's law and a part σ^{ne} at the ruptured sites where linear elasticity is violated. It is straightforward to see that for one rupture at $\boldsymbol{r}_0$ we have

$$D_j \sigma_{xj}^{el}(\boldsymbol{r}) + \sigma^{ne} D_y(\delta_{\boldsymbol{r},\boldsymbol{r}_o}) = 0 \tag{2.6}$$

$$D_j \sigma_{yj}^{el}(\boldsymbol{r}) + \sigma^{ne} D_x(\delta_{\boldsymbol{r},\boldsymbol{r}_o}) = 0. \tag{2.7}$$

Given σ^{ne} we can obtain a solution for σ^{el}, which then can be used to obtain σ^{ne} self consistently by applying the boundary condition at the ruptured site.

In the case of multiple ruptures along the x direction at the locations $\{\boldsymbol{r}_i\}$ with $i = 1, \ldots, n_r$, the additional shear stress, $\sigma_{xy}(\boldsymbol{r})$, and displacement, $u_x(\boldsymbol{r})$, can be written as follows:

$$\sigma_{xy}'(\boldsymbol{r}) = \alpha_\sigma \sum_{i=1}^{n_r} [f_i(\boldsymbol{r}_i) G_\sigma(\boldsymbol{r} - \boldsymbol{r}_i)] \tag{2.8}$$

$$u'_x(\boldsymbol{r}) = \alpha_u \left\{ \sum_{i=1}^{n_r} f_i(\boldsymbol{r}_i)[\gamma G_{u1}(\boldsymbol{r}-\boldsymbol{r}_i) + G_{u2}(\boldsymbol{r}-\boldsymbol{r}_i)] \right\} \tag{2.9}$$

where $f_i(\boldsymbol{r}_i)$ denotes σ^{ne} at $\boldsymbol{r}_i$, $\alpha_\sigma = (K+\mu/3)/(K+4\mu/3)$, $\alpha_u = \alpha_\sigma/\mu$, and $\gamma = \mu/(K+\mu/3)$. The Green functions can be worked out following [3]:

$$G_\sigma(\boldsymbol{r}) = \int_{-\pi}^{\pi} \frac{\mathrm{d}k_x}{2\pi} \int_{-\pi}^{\pi} \frac{\mathrm{d}k_y}{2\pi} \frac{\sin^2 k_x \sin^2 k_y}{(1-\cos k_x \cos k_y)^2} \mathrm{e}^{\mathrm{i}\boldsymbol{k}\cdot\boldsymbol{r}} \tag{2.10}$$

$$G_{u1}(\boldsymbol{r}) = \mathrm{i} \int_{-\pi}^{\pi} \frac{\mathrm{d}k_x}{2\pi} \int_{-\pi}^{\pi} \frac{\mathrm{d}k_y}{2\pi} \frac{\sin\frac{k_y}{2}\cos\frac{k_x}{2}}{1-\cos k_x \cos k_y} \mathrm{e}^{\mathrm{i}\boldsymbol{k}\cdot\boldsymbol{r}} \tag{2.11}$$

and

$$G_{u2}(\boldsymbol{r}) = \mathrm{i} \int_{-\pi}^{\pi} \frac{\mathrm{d}k_x}{2\pi} \int_{-\pi}^{\pi} \frac{\mathrm{d}k_y}{2\pi} \frac{(\cos k_x - \cos k_y)\sin\frac{k_y}{2}\cos\frac{k_x}{2}}{(1-\cos k_x \cos k_y)^2} \mathrm{e}^{\mathrm{i}\boldsymbol{k}\cdot\boldsymbol{r}}. \tag{2.12}$$

It is worth noting that with the discretization defined in equations (2.4) and (2.5) the Laplacian in k-space is given by $2(1-\cos k_x \cos k_y)$. In the following we find it convenient to redefine $\alpha_\sigma f_i$ as f_i and scale the displacement u_x, u'_x by a factor of μ; this removes the factors α_σ and α_u in equations (2.8) and (2.9):

$$\sigma'_{xy}(\boldsymbol{r}) = \sum_{i=1}^{n_r} [f_i(\boldsymbol{r}_i) G_\sigma(\boldsymbol{r}-\boldsymbol{r}_i)] \tag{2.13}$$

$$u'_x(\boldsymbol{r}) = \sum_{i=1}^{n_r} f_i(\boldsymbol{r}_i)[\gamma G_{u1}(\boldsymbol{r}-\boldsymbol{r}_i) + G_{u2}(\boldsymbol{r}-\boldsymbol{r}_i)]. \tag{2.14}$$

A straightforward implementation of the quasistatic fracture process used in [3] is to consider a sequence of ruptures at the locations where the stresses exceed the corresponding thresholds. There are a few problems associated with this simple implementation: the ruptures occur at the corners of plaquettes which is not physically appealing if these unit plaquettes are interpreted as real physical blocks. In addition, there is a degeneracy problem associated with the direction of ruptures: a given local rupture (generated when σ_{xy} exceeds the threshold), can be interpreted either as a rupture along the x or y direction. More troublesome is the fact that the rupture at the position $\boldsymbol{r}_0$ does not change the stress at the positions $\boldsymbol{r}_0 + m\hat{e}_x + n\hat{e}_y$ when $m+n$ is an odd integer; this problem of sublattice decoupling is obviously an artefact of this discretization scheme. We need a better discretization scheme to avoid the above problems. One way this can be achieved is by using a coarse-grained lattice with a new unit cell consisting of four unit cells on the original lattice as illustrated in figure 1. The coarse-grained displacement and stress fields will be discussed first. We define a coarse-grained displacement (denoting this by a bar) at the centre of the new cell as

$$\bar{u}_i(\boldsymbol{r}) = \frac{1}{4}\left[u_i\left(\boldsymbol{r} - \frac{\hat{e}_x}{2} - \frac{\hat{e}_y}{2}\right) + u_i\left(\boldsymbol{r} - \frac{\hat{e}_x}{2} + \frac{\hat{e}_y}{2}\right) + u_i\left(\boldsymbol{r} + \frac{\hat{e}_x}{2} - \frac{\hat{e}_y}{2}\right) + u_i\left(\boldsymbol{r} + \frac{\hat{e}_x}{2} + \frac{\hat{e}_y}{2}\right)\right] \tag{2.15}$$

the new stress is defined at the centre of the interface of the new cells with its value being the average stress along the interface. For the shear stress, σ_{xy}, along the horizontal interface we define

$$\bar{\sigma}_{xy}(\boldsymbol{r}) = \tfrac{1}{4}[\sigma_{xy}(\boldsymbol{r}-\hat{e}_x) + 2\sigma_{xy}(\boldsymbol{r}) + \sigma_{xy}(\boldsymbol{r}+\hat{e}_x)]. \tag{2.16}$$

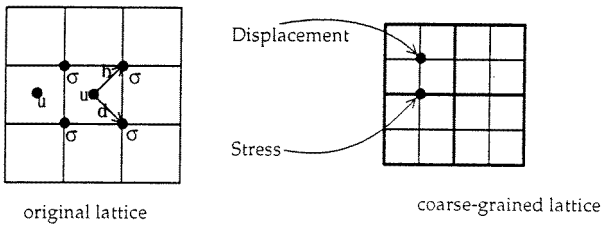

Figure 1. In the original lattice on the left the stress tensor (σ) resides at the corners and the displacement (u) at the centres of the plaquettes. The coarse-grained plaquette is shown on the right with the original lattice shown by light lines and the new lattice by heavy lines.

We next rewrite equations (2.8) and (2.9) in terms of the coarse-grained variables. This requires that we define a rupture in the new lattice in terms of the ruptures on the original lattice: a rupture in the new lattice at $\boldsymbol{r}_0$ with the double-couple strength $\bar{f}$ corresponds to ruptures in the original lattice at $\boldsymbol{r}_0 - \hat{e}_x$ (with double-couple strength $\bar{f}/4$), $\boldsymbol{r}_0$ (with $\bar{f}/2$), and $\boldsymbol{r}_0 + \hat{e}_x$ (with $\bar{f}/4$). Now the Green functions for the coarse-grained lattice can be obtained as follows. Dropping the subscripts xy and x in σ_{xy} and u_x for convenience, the additional stress on the coarse-grained lattice due to the rupture is given by

$$\bar{\sigma}'(\boldsymbol{r}) = \tfrac{1}{4}[\sigma'(\boldsymbol{r} - \hat{e}_x) + 2\sigma'(\boldsymbol{r}) + \sigma'(\boldsymbol{r} + \hat{e}_x)].$$

The additional stress on the original lattice can be obtained using equation (2.13):

$$\sigma'(\boldsymbol{r}) = \frac{\bar{f}}{4}[G_\sigma(\boldsymbol{r} - \boldsymbol{r}_0 - \hat{e}_x) + 2G_\sigma(\boldsymbol{r} - \boldsymbol{r}_0) + G_\sigma(\boldsymbol{r} - \boldsymbol{r}_0 + \hat{e}_x)].$$

We thus have

$$\bar{\sigma}'(\boldsymbol{r}) = \bar{f}\bar{G}_\sigma(\boldsymbol{r} - \boldsymbol{r}_0) \tag{2.17}$$

where

$$\bar{G}_\sigma(\boldsymbol{r}) = \tfrac{1}{16}[G_\sigma(\boldsymbol{r} - 2\hat{e}_x) + 4G_\sigma(\boldsymbol{r} - \hat{e}_x) + 6G_\sigma(\boldsymbol{r}) + 4G_\sigma(\boldsymbol{r} + \hat{e}_x) + G_\sigma(\boldsymbol{r} + 2\hat{e}_x)]. \tag{2.18}$$

The additional displacement along the x direction in the new lattice is given by

$$\bar{u}'(\boldsymbol{r}) = \frac{1}{4}\left[u'\left(\boldsymbol{r} - \frac{\hat{e}_x}{2} - \frac{\hat{e}_y}{2}\right) + u'\left(\boldsymbol{r} - \frac{\hat{e}_x}{2} + \frac{\hat{e}_y}{2}\right) + u'\left(\boldsymbol{r} + \frac{\hat{e}_x}{2} - \frac{\hat{e}_y}{2}\right) + u'\left(\boldsymbol{r} + \frac{\hat{e}_x}{2} + \frac{\hat{e}_y}{2}\right)\right] \tag{2.19}$$

where

$$u'(\boldsymbol{r}) = \frac{\bar{f}}{4}[\gamma(G_{u1}(\boldsymbol{r} - \boldsymbol{r}_0 - \hat{e}_x) + 2G_{u1}(\boldsymbol{r} - \boldsymbol{r}_0) + G_{u1}(\boldsymbol{r} - \boldsymbol{r}_0 + \hat{e}_x)) + (G_{u2}(\boldsymbol{r} - \boldsymbol{r}_0 - \hat{e}_x) + 2G_{u2}(\boldsymbol{r} - \boldsymbol{r}_0) + G_{u2}(\boldsymbol{r} - \boldsymbol{r}_0 + \hat{e}_x))]. \tag{2.20}$$

Substituting the above expression for $u'(\boldsymbol{r})$ into equation (2.19) we obtain

$$\bar{u}'(\boldsymbol{r}) = \bar{f}[\gamma\bar{G}_{u1}(\boldsymbol{r} - \boldsymbol{r}_0) + \bar{G}_{u2}(\boldsymbol{r} - \boldsymbol{r}_0)] \equiv \bar{f}G_u(\boldsymbol{r} - \boldsymbol{r}_0) \tag{2.21}$$

where the coarse-grained Green functions can be written as

$$\bar{G}_{u1,2}(\boldsymbol{r}) = \frac{1}{2}\left[\tilde{G}_{u1,2}\left(\boldsymbol{r} - \frac{\hat{e}_y}{2}\right) + \tilde{G}_{u1,2}\left(\boldsymbol{r} + \frac{\hat{e}_y}{2}\right)\right]$$

with

$$\tilde{G}_{u1,2}(\boldsymbol{r}) = \frac{1}{8}\Big[G_{u1,2}\left(\boldsymbol{r} - \frac{3\hat{e}_x}{2}\right) + 3G_{u1,2}\left(\boldsymbol{r} - \frac{\hat{e}_x}{2}\right) + 3G_{u1,2}\left(\boldsymbol{r} + \frac{\hat{e}_x}{2}\right) + G_{u1,2}\left(\boldsymbol{r} + \frac{3\hat{e}_x}{2}\right)\Big].$$

In the numerical procedure for studying quasistatic processes of fractures, it is more efficient to compute the Green functions and store them so that they can be used repeatedly to calculate stress redistribution when new ruptures occur or when there is a change in the boundary conditions. It is important to have an efficient method to accurately calculate the Green functions numerically. Achieving the necessary precision by directly evaluating the expressions, for example in equation (2.10) which involves performing a two-dimensional integral for each position $\boldsymbol{r}$, is very time consuming. We have successfully reduced the two-dimensional integrals to one-dimensional integrals, using the fact that the integrals need only be done for points with integer or half-integer coordinates; this leads to an efficient method for calculating Green functions. The method can also be used to calculate Green functions involved in other breakdown problems. The calculation in appendix A leads to the following result for $y \geqslant 0$

$$G_\sigma(x, y) = \int_0^\pi \frac{\mathrm{d}k_x}{\pi} |\sin k_x| \cos k_x x \left[\frac{z_1^y}{1 + |\sin k_x|} - \eta(y)\frac{|\sin k_x| z_1^{y-2}}{(1 + |\sin k_x|)^2}\right] \tag{2.22}$$

where $z_1 = (1 - |\sin k_x|)/\cos k_x$, $\eta(y) = y - 1$ if $y > 1$ and $\eta(y) = 0$ when $y = 0, 1$. For the case that $y < 0$ the Green function can be obtained using the symmetry relation

$$G_\sigma(\pm x, \pm y) = G_\sigma(x, y). \tag{2.23}$$

We can use the same idea to evaluate $G_{u1,2}$ (for x and y half-integers). For the case $y > 0$ we have obtained

$$G_{u1}(x, y) = -\int_0^\pi \frac{\mathrm{d}k_x}{\pi} \frac{\cos k_x x z_1^{y-1/2}}{2\left(\left|\cos\frac{k_x}{2}\right| + \left|\sin\frac{k_x}{2}\right|\right)} \tag{2.24}$$

and

$$G_{u2}(x, y) = -\int_0^\pi \frac{\mathrm{d}k_x}{\pi} \frac{\cos\frac{k_x}{2}\cos k_x x\left[\left(y + \frac{1}{2}\right) z_1^{y-1/2} - \left(y - \frac{1}{2}\right) z_1^{y-3/2}\right]}{2(1 + |\sin k_x|)}. \tag{2.25}$$

For the case that $y < 0$, the following symmetry relations

$$G_{u1,2}(\pm x, -y) = -G_{u1,2}(\pm x, y) \tag{2.26}$$

can be used to evaluate the Green functions.

The Green function for the coarse-grained lattice can now be calculated in a straightforward way using

$$\bar{G}_\sigma(\boldsymbol{r}) = \int_0^\pi \frac{\mathrm{d}k_x}{\pi} |\sin k_x| \cos^4\frac{k_x}{2} \cos k_x x \left[\frac{z_1^y}{1 + |\sin k_x|} - \eta(y)\frac{|\sin k_x| z_1^{y-2}}{(1 + |\sin k_x|)^2}\right] \tag{2.27}$$

$$\bar{G}_{u1}(\boldsymbol{r}) = -\frac{1}{4}\int_0^\pi \frac{\mathrm{d}k_x}{\pi} \frac{\cos^3\frac{k_x}{2}\cos k_x x(1 + z_1) z_1^{y-1}}{\left|\cos\frac{k_x}{2}\right| + \left|\sin\frac{k_x}{2}\right|} \tag{2.28}$$

and

$$\bar{G}_{u2}(\boldsymbol{r}) = -\frac{1}{4}\int_0^\pi \frac{\mathrm{d}k_x}{\pi} \frac{\cos^4\frac{k_x}{2}\cos k_x x[(y + 1) z_1^y - (y - 1) z_1^{y-2}]}{1 + |\sin k_x|}. \tag{2.29}$$

Note that the lattice spacing of the coarse-grained lattice is two in units of the original lattice. We rescale the length by half for convenience so that the coarse-grained lattice has unit spacing. This can be done by replacing both x and y by $2x$ and $2y$ respectively in the coarse-grained Green functions. From now on we restrict our attention to the coarse-grained lattice and therefore, we will drop the bars in $\bar{G}_{\sigma,u1,u2}$ for notational simplicity. We rewrite the results below: the Green function for the stress is given by

$$G_\sigma(\boldsymbol{r}) = \int_0^\pi \frac{\mathrm{d}k_x}{\pi} |\sin k_x| \cos^4 \frac{k_x}{2} \cos 2k_x x \left[\frac{z_1^{2y}}{1+|\sin k_x|} - \eta(2y) \frac{|\sin k_x| z_1^{2y-2}}{(1+|\sin k_x|)^2} \right] \tag{2.30}$$

where both x and $y \geqslant 0$ are integers; G_σ for $y < 0$ can be obtained by the symmetry relation, that is the same as the one for the Green function of the original lattice (see equation (2.23)). The Green function for the displacement are given by

$$G_{u1}(\boldsymbol{r}) = -\frac{1}{4} \int_0^\pi \frac{\mathrm{d}k_x}{\pi} \frac{\cos^3 \frac{k_x}{2} \cos 2k_x x (1+z_1) z_1^{2y-1}}{\left|\cos \frac{k_x}{2}\right| + \left|\sin \frac{k_x}{2}\right|} \tag{2.31}$$

and

$$G_{u2}(\boldsymbol{r}) = -\frac{1}{4} \int_0^\pi \frac{\mathrm{d}k_x}{\pi} \frac{\cos^4 \frac{k_x}{2} \cos 2k_x x [(2y+1) z_1^{2y} - (2y-1) z_1^{2y-2}]}{1+|\sin k_x|} \tag{2.32}$$

where x is an integer and y is a half-integer; $G_{u1,2}$ for $y < 0$ can again be obtained by the symmetry relations. We will use these Green functions in our simulations.

The self-consistent numerical procedures are based on equations (2.13) and (2.14), where the boundary conditions (external boundary conditions or internal boundary conditions at the ruptured sites) give rise to self-consistency conditions for the double-couple strengths. The boundary conditions at the ruptures can either be expressed in terms of the local stress (e.g. the stress at the ruptured surface is reduced to zero), or local displacement (when the ruptured surface is stuck the displacements on the two sides are equal), or both. The self-consistency equations can then be solved for the double-couple strengths, which in turn are used to obtain the stress and displacement distribution in the system. The key step in the simulation is the self-consistent determination of the double-couple strengths, given the external boundary conditions and internal fracture conditions, which are constantly changing as new fractures are being generated. Typically, in our simulations, the double-couple strengths are obtained incrementally, i.e. we determine the additional double-couple strengths required to satisfy the self-consistency conditions as the external boundary conditions and the internal fracture pattern change; we can then compute the new stress and displacement in the system.

As an illustration of the self-consistent technique, consider the following calculation of the build-up of the stress near a locked fault segment in an infinite seismic zone. The fault line is the horizontal line at the middle of the system, and the stuck segment extends from $x = 0$ to $x = L - 1$ (we take $L = 100$). The top and bottom plates move relative to each other, and the boundary condition is given by $u(x, y = \infty) - u(x, y = -\infty) = \Delta u$ (Δu is set to 1 in the calculation). When there is no stuck segment, the solution is simple ($u(x, y) = 0.5\mathrm{sign}(y)$ and the system is stress free, $\sigma(x, y) = 0$). However, since the fault segment is stuck, there will be a stress build-up in its vicinity. The extra stress can be calculated by evaluating the extra double-couple strengths along the fault required to enforce the condition of zero relative displacement along the stuck fault segment. Let $f(x)$ be the extra double-couple strength required at the position $(x, 0)$ of the fault. We can then

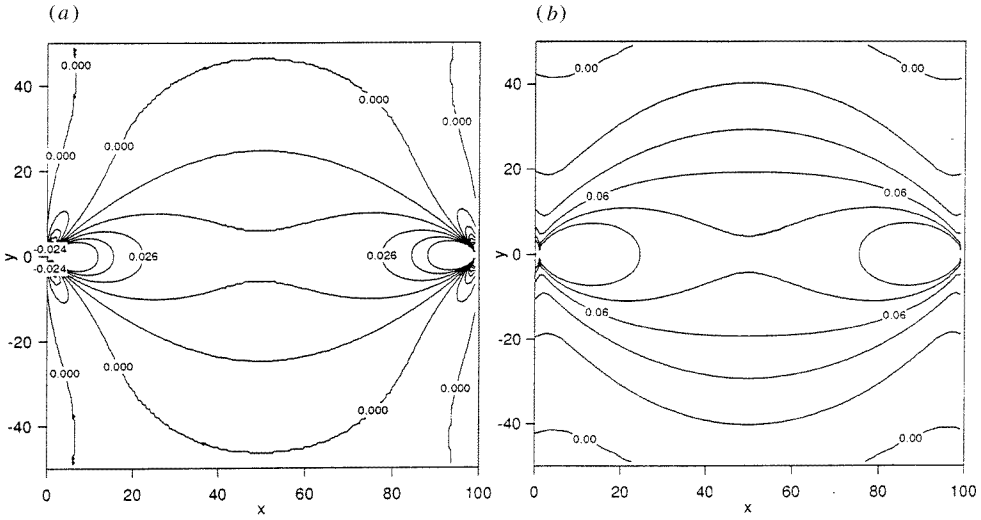

Figure 2. Comparison of the stress distributions. (*a*) Shows a stuck fault segment between 0 and 100 ignoring the region outside the zone. (*b*) Shows free stress boundary conditions are employed on a fault segment of length 25 extending on either side at $y = 0$.

write down the stress and displacement of the system as

$$u(x, y) = 0.5\,\mathrm{sign}(y) + \sum_{x'} f(x')G_u(x - x', y)$$
$$\sigma(x, y) = \sum_{x'} f(x')G_\sigma(x - x', y). \tag{2.33}$$

The boundary condition on the stuck fault segment implies that

$$u(x, \tfrac{1}{2}) - u(x, -\tfrac{1}{2}) = 0 \tag{2.34}$$

for $x = 0$ to $L - 1$. These conditions are used to determine the additional double-couple strengths, $f(x)$, self-consistently. Note that we should in principle solve for the additional double-couple strengths along the entire fault (instead of just the stuck fault segment), but this is not possible numerically. Instead, we first make the approximation of ignoring the additional double-couple strengths outside the stuck fault segment; the above conditions on the stuck fault segment are sufficient to determine the additional double-couple strengths $f(x)$ for $x = 0$ to $x = L - 1$, from which the additional stresses and displacements in the system can be evaluated via equation (2.33). We have obtained an estimate of the effect of the above approximation by including some additional double-couple strengths outside the stuck segment and applying zero-stress boundary conditions on these segments; the results are presented in figure 2. Figure 2(*a*) is the contour plot of the additional stress due to the stuck fault segment at $0 \leqslant x < 100$; the calculation is done by ignoring the additional double-couple strengths outside of the fault segment. Figure 2(*b*) shows the same stress distribution, with the calculation done including some additional double-couple strengths outside of the stuck fault segment. In this case, the self-consistent calculation is done for the double-couple strengths on the extended segment $-50 \leqslant x < 150$. As can be seen from the figures, there are significant differences between the stress distributions near the edges of the stuck segment, as we would expect. However, the overall stress pattern away from the edges is similar.

3. Numerical procedure for simulating quasistatic process of fractures

In this section we will present some new numerical techniques for the efficient simulation of quasistatic models of fractures. Recall that in a typical model, we consider a discrete, elastic medium with local stress thresholds; ruptures occur when the actual local stresses exceed the corresponding thresholds. The system is driven, typically, by gradual changes in the external boundary conditions, e.g. by increasing the external stress or the relative displacements at the external boundaries. The driving of the system causes the stress to increase in the system (the build-up is not necessarily uniform, as can be seen in the example studied in the last section), resulting in ruptures in the system. The quasistatic process consists of periods in which there are sequences of ruptures, separated by 'rest periods' when all the stresses are below their corresponding thresholds. During the 'rest period', the stress is accumulating in the system due to continual external driving. The external boundary conditions are held fixed (a basic assumption of quasistatic models) during a sequence of ruptures. This corresponds to the separation of time scales inherent in the system between the response time and the much longer time scale characteristic of the external drive. This separation of time scales is believed to be one of the distinguishing features of the phenomenon of self-organized criticality that leads to scale-invariant behaviour [13].

We now discuss the calculation in greater detail. The stress distribution has to be recalculated either because new ruptures occur causing stress redistribution in response to it or because of the external driving; the new stress distribution determines if further ruptures will be generated in the system. The case of the change in stress due to the external drive is simple. Since the additional stress is linearly proportional to the external driving, it is easy to calculate the additional driving required to generate a new rupture in the system. Let $\sigma^{\text{old}}(\boldsymbol{r})$ be the distribution of stress immediately after the last sequence of ruptures, and let $\sigma'(\boldsymbol{r})$ be the additional stress generated when the parameter, p, that characterizes the drive (depending on the external boundary condition used, p can be the external stress, the external displacement or the time spent in the accumulation process) is increased by unit magnitude. The new stress when the parameter is increased by Δp is given by $\sigma^{\text{new}}(\boldsymbol{r}) = \sigma^{\text{old}}(\boldsymbol{r}) + \Delta p\sigma'(\boldsymbol{r})$. It is easy from this formula to calculate the value of Δp required to generate the first rupture in the next sequence of ruptures, by finding the minimum Δp required such that $|\sigma^{\text{new}}(\boldsymbol{r})|$ reaches the threshold at one site in the system.

After the first rupture, a new sequence of ruptures starts during which p is assumed fixed. The first rupture changes the stress distribution of the system; this in turn may cause stresses in some locations to exceed the corresponding thresholds and new ruptures in these locations will be generated. The new ruptures further change the stress distribution of the system and may cause additional ruptures and so on. The process continues until all the stresses are below their corresponding thresholds and the system then enters another 'rest period'. Both the stress change in the 'rest period' and the stress redistribution within the sequence of ruptures are calculated using the self-consistent method discussed in the previous section. A straightforward formulation of the problem leads to a calculation involving the solution of a set of linear equations for the double-couple strengths directly at each step of the simulation. The equation assumes the form

$$\sum_j A_{ij} f_j = b_i \tag{3.1}$$

where A is an $N \times N$ matrix with N being the number of double couples, and the matrix elements of A are the values of the appropriate Green functions. The vector, f, contains the double-couple strengths, which we want to obtain from the equations. The vector, b,

depends on the external boundary conditions and the boundary conditions imposed at the ruptured sites. For example, let i_0 denote the position of a newly ruptured site; let us impose the boundary condition that the stress at the site is reduced to zero after the rupture, the external boundary condition remaining unchanged. Then the matrix element $A_{i_0 j}$ is given by $G_\sigma(\boldsymbol{r}_{i_0} - \boldsymbol{r}_j)$ and b_{i_0} is given by $-\sigma^{\text{old}}(\boldsymbol{r}_{i_0})$ ($\sigma^{\text{old}}(\boldsymbol{r}_{i_0})$ is the stress at i_0 just before the rupture) so that the new stress is fixed to zero. If, on the other hand, i_0 is a site on a stuck segment of the fault, then $A_{i_0 j}$ will be related to the Green functions for the displacement: $A_{i_0 j} = G_u(\boldsymbol{r}_{i_0} + \hat{e}_y/2 - \boldsymbol{r}_j) - G_u(\boldsymbol{r}_{i_0} - \hat{e}_y/2 - \boldsymbol{r}_j)$ and the corresponding b_{i_0} is zero (if there are no changes in the external boundary conditions).

Since there are usually only a few new ruptures generated at each step of the simulation, most of the matrix elements of A remain unchanged. This fact can be used to construct a more efficient numerical procedure for simulating the quasistatic process than the method of directly solving the linear equation at each step. The idea is to keep a copy of the current matrix B which is the inverse of A. The matrix B is updated at each step, and the solution for the double-couple strengths is obtained using $f = Bb$. The number of operations in the computation involved in updating B, scales as the $N^2 n$, where n is the number of new ruptures. If n is much smaller than N, as is usually the case, then this method is much more efficient than the straightforward method of solving the linear equation directly, which requires a computation of the order of N^3. The details are described in appendix B. The numerical techniques described in appendix B for solving the consecutive set of linear equations that arise in the simulation of the quasistatic fracture process, can also be used in the simulation of quasistatic processes of other breakdown problems in which the self-consistent procedure based on the Green function approach can also be used. In the following section, however, this technique is used to study an earthquake model with a pre-existing fault in the seismic zone.

4. A model of seismic zone with a pre-existing fault

Model studies of earthquakes have abounded in the last few years. It must be stressed at the outset that the phenomenological information about seismic zones that has been accumulated is extensive [12] but it is not feasible numerically to incorporate all the details. The approach is to simplify the full three-dimensional elastodynamic equations that are well accepted in different ways. In addition, the appropriate boundary conditions at the ruptures and the time scale on which they should change, due to the presence of fluids, thermal processes etc and the role of disorder, remain controversial and different approximations have been adopted. The modelling by physicists has typically focused first on statistical aspects. It is convenient to divide these models into two classes: quasistatic or dynamic. The motivation for the former is roughly as follows. The dynamics during an earthquake is complex and involves rupture propagation, seismic waves, stick–slip friction and energy dissipation. However, the duration of an earthquake is much smaller than the time scale of the stress build-up in the seismic zone. This feature has lead several researchers to consider quasistatic models that ignore short-time dynamics and focus on the long-time statistical behaviour of earthquakes. Over the past few years, such quasistatic versions of spring-block models, originally suggested by Burridge and Knopoff [14] to study the stick–slip dynamics at the faults, have been studied [15–21] in the context of 'self organized criticality' [22]. On the other hand, there have been several studies of *dynamical* mechanical fault models: one class of models include frictional forces with features such as velocity weakening but without disorder focusing on the fault in one dimension [24, 26] and in two dimensions [25]; more recently, there has been an investigation of a slip-weakening mechanism [27].

Models that include radiation damping have also been considered [28]. However, all these models limit themselves to local, often near-neighbour, redistribution of the stress and often consider only a single fault. All these studies, quasistatic and dynamic, being conceptually simple, nicely demonstrate the emergence of scaling behaviour; in particular, they have been shown to yield, typically numerically, the Gutenberg–Richter power law [23] for the frequency-size distributions.

While some of the quasistatic stick–slip models capture several features of earthquakes, most of them do not explicitly include long-ranged redistribution of the elastic stress following a slip event [29]. An important study that does consider the evolution of a portion of the San Andreas fault plane uses continuum Green functions and slowly varying boundary conditions associated with the seismicity in other parts of the fault region [30]. Quasistatic models that consider 'dislocations' instead of 'cracks' have also been investigated [16].

It is worth noting that the other standard numerical approaches to fracture processes are difficult to implement in earthquake models. Molecular dynamics techniques are useful at the microscopic level but are computationally too expensive to study a medium with many cracks. The powerful and widely used finite element method, on the other hand, requires elements much smaller than the cracks and the size of the heterogeneities. This renders the finite element method difficult to use in the study of a heterogeneous medium with many microcracks.

We discuss briefly the motivation behind our model whose origins are in the paper by Chen *et al* [31]. The seismic zone typically contains faults with complex spatial patterns and fractal geometry [32]. Tectonic loading of the seismic zone causes the plates on either side of the fault to move in opposite directions; the consequent build-up of the stress leads to an earthquake consisting of rupture processes that include stick–slip behaviour at pre-existing fault structures and the formation of new cracks in the seismic zone possibly creating new fault segments [12]. The study of the spatial characteristics of earthquakes, therefore, requires a model for the entire seismic zone with embedded pre-existing fault structures. Therefore, we have studied quasistatic models that include redistribution of the long-ranged elastic stresses. However, they do not include dynamical phenomena. In our previous paper [11], a simple model incorporating a pre-existing fault was proposed and studied. The model, however, was implemented with the dipole representation of ruptures for simplicity; this representation does not incorporate the full tensorial nature of the elastic forces. We note that the requirement after a local shear rupture neither an additional force nor an additional torque can be generated. This means that the rupture must be modelled by a double-couple or quadrupolar force distribution [4]. In this section we present the double-couple version of the model. Thus, computationally, the essential difference between the current model and that of our previous paper lies in the use of the double-couple Green functions. There is also a difference in the choice of the boundary conditions for ruptured surfaces which will be discussed shortly. One of our conclusions is that the results for the scaling of the distribution of earthquakes remain unaffected by the inclusion of double-couple forces; within the limitations of our numerical calculations it is tempting to conjecture universality of this class of models.

As in [11], we consider a two-dimensional model with a linear vertical strike–slip fault. The basic ideas and methods presented here are not limited to this specific model and can be generalized to study seismic zones with more complex fault geometries and zone boundaries. The seismic zone is modelled using a $L_x \times L_y$ lattice of blocks $a_x \times a_y \times a_z$, where a_z is the thickness of the crust; each block can be considered to have a characteristic size of a few kilometers, and a_z is assumed to be constant. Embedded in the middle of the zone is a linear strike–slip fault along the x direction. The displacements are assumed to

be small compared to the size of the block.

Tectonic loading of the seismic zone is represented by the driving of the plates on both sides of the fault in opposing directions: the plate on one side of the fault (positive y) is assumed to move to the right (positive x) with a speed $v_0/2$ while the other plate moves to the left with the same speed, leading to a relative velocity v_0 for the plate motion. The mechanism for earthquakes in the model is as follows. The blocks on one side of the *fault* experience frictional forces due to the blocks on the other side, resulting in a zero relative displacement at the fault, i.e. the fault surfaces are stuck while there is slow relative motion of the tectonic plates during the quiescent periods between earthquakes. As was shown in section 2, this causes stress to build up in the vicinity of the fault. Earthquakes are then caused by faulting instabilities such as *shear ruptures* in the zone or *slips* at the fault surfaces when the stress (or frictional force) exceeds the appropriate local threshold value.

In addition to v_0, which sets the time scale for measuring the time interval between successive earthquakes, we introduce three local parameters in our model. The stress thresholds between adjacent blocks are distributed uniformly and randomly between a maximum threshold, σ_u, and a minimum threshold, σ_l; we also define an arrest stress, σ_a, to sites that are ruptured; the three quantities obey $\sigma_u \geqslant \sigma_l \geqslant \sigma_a$. The non-uniformities in the thresholds can be viewed as a simple way of incorporating the spatial inhomogeneities and the variations in the material properties of the seismic medium. One can easily introduce spatial correlations in thresholds and model specific seismic zones for which information is available.

An earthquake in our model is a sequence of ruptures in a quasistatic process described in the previous section. The boundary conditions that were employed were as follows. During the earthquake, which occurs on a rapid time scale, the plates are assumed to be held fixed, i.e. there is no change in the external boundary conditions; the new shear stress at the ruptured sites are set to $\sigma^{\text{new}} = \sigma_a$ during the remaining steps of the earthquake†; the sites on the fault segment that have not ruptured during that particular earthquake continue to remain stuck. These conditions cause stress redistribution and the earthquake can proceed in several steps after the initiation. The stress distribution in the seismic zone after each step is obtained self consistently using the procedure described in the previous sections. The earthquake ends when the stress field reaches a state that is below the threshold everywhere. After each earthquake, ruptures in the seismic zone are healed (i.e. no new faults are generated in the zone; the healing time is assumed to be much smaller than the time scale for stress build-up), while the surfaces along the fault are treated with stuck boundary conditions again. In the numerical simulation, the matrix B is initialized, at the end of each earthquake, to the inverse of the matrix A_0 corresponding to the boundary condition of a stuck fault segment at $0 \leqslant x < L_x$ and no ruptures off the faults. The matrix B is updated using the methods described in the previous section. This numerical procedure is much faster than the one used in [11].

One can consider a variety of choices for the parameters $\sigma_{u,l,a}$. For simplicity, we fix $\sigma_a = 0.1$ and $\sigma_u = 1.0$. The simulations are done for different values of σ_l. After each earthquake the stress threshold at the ruptured sites can either be reset to a new value signifying a change in strength at the ruptured/slipped sites, or be fixed for the entire evolution. The latter corresponds to quenched disorder and leads to a deterministic evolution for the system. For the purpose of illustration, we mainly discuss the former case here and

† In the model of our previous paper [11], the previously ruptured surfaces become stuck in the remaining steps of the earthquakes. This choice of the internal boundary condition causes unphysical rupturing of the whole system. Nevertheless, fixing the stress at the ruptured site to the value of the arrest stress appears to be more physically meaningful; the ruptured sites can keep slipping during the earthquake.

report results for the quenched case.

To characterize earthquakes in our model, we use the same expressions for the energy released (E) and seismic moment (M_0) defined in [11]: $E \approx \sum_i [u_{xi}](\sigma^{\text{old}}(i) - \sigma^{\text{new}}(i))$ and $M_0 \approx \mu |\sum_i [u_{xi}]|$, where the displacement discontinuity ($[u_x]$) is the difference in the displacement of blocks on either side of the rupture/slip, $(\sigma^{\text{old}} - \sigma^{\text{new}})$ is the stress drop during the earthquake, and the sum is over all the surfaces that slip or rupture.

We first present the spatial features of earthquakes in our model. The global stick–slip behaviour of the model is illustrated in the displacement field $u_x^{\text{extra}}(x, y)$ during an earthquake. Figure 3 shows this for a fixed x as a function of y due to a large earthquake that occurred at the fault. The slip at the fault displays a well known feature of large earthquakes observed in surface faulting (see e.g. [33]). Moreover, the average slip rate at the fault agrees with the relative plate velocity. We also find that most of the earthquakes occur in the vicinity of the fault.

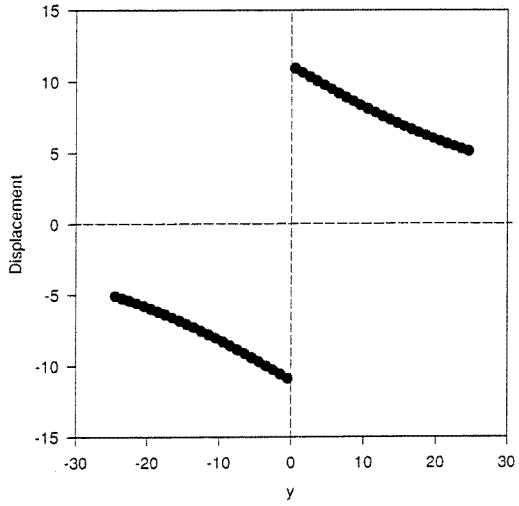

Figure 3. The displacement field (full circles), as a function of y for a fixed x, due to a slip (displacement discontinuity) at the fault ($y = 0$) in a large earthquake.

Next, we present statistical features of earthquakes in the evolution of the model by using an 80×50 system with 50 000 earthquakes after skipping the first 10 000 (so that the system reaches a statistically stationary state [22]). In figure 4(a) we display log–log plots of the distribution $P(E)$ versus E for $\sigma_l = 0.1001$; the linear portion which extends up to $\bar{E}$ corresponds to a power law $P(E) \approx E^{-1-\beta}$ with $\beta = 0.7 \pm 0.1$. The corresponding plot, $P(M_0)$, for the seismic moment distribution is shown in figure 4(b); the exponent for the scaling is found to be roughly the same as in the energy distribution $P(E)$. We have also obtained the size distribution for $\sigma_l = 0.4$, 0.7, and 1.0. Similar scaling behaviours are obtained except for the case $\sigma_l = 1.0$ (all thresholds are equal, i.e. no spatial inhomogeneities), where no scaling is found: the system appears to evolve to a periodic state. This suggests that some spatial inhomogeneity is important for obtaining scaling in this class of models. Nevertheless, the scaling appears not to depend on the degree of spatial inhomogeneities in the model. In addition, we have also considered deterministic evolution of the model (the thresholds are spatially inhomogeneous, but are fixed in the entire simulation, i.e. the disorder is quenched), and we find the *same* scaling behaviours. The exponent obtained here is similar to that of model A in [11], and is consistent with the

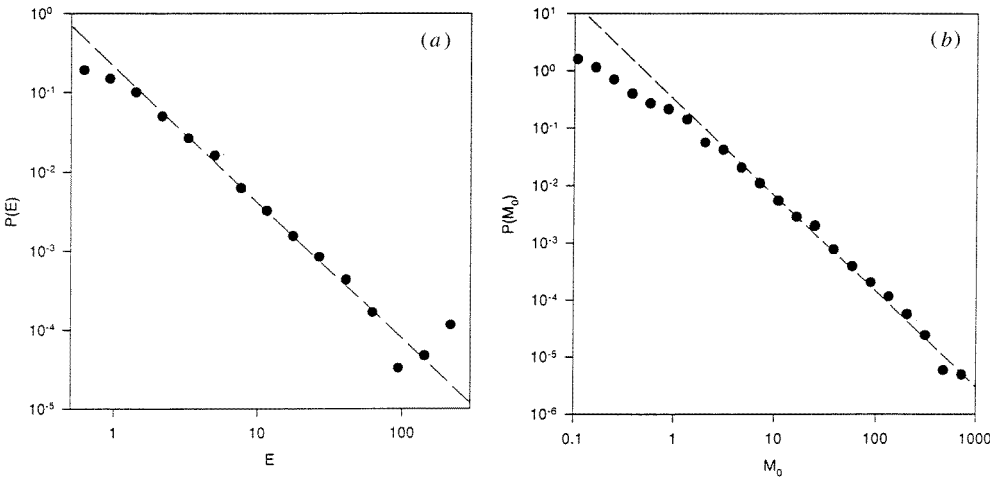

Figure 4. Log–log plot of the probability of earthquakes (for a sequence of 50 000 quakes on an 80×50 system) versus (a) the energy released, E, and (b) the seismic moment, M_0. Both correspond to power laws with an exponent 0.7 ± 0.1.

seismological data gathered over the past 100 years [34] as discussed in our earlier paper [10].

In the calculation above, we have neglected the changes in the double-couple strengths (on the fault) outside the stuck fault segment $0 \leqslant x < L_x$. To check the effect of this approximation to the scaling law, we include some double-couple strengths beyond the edges of the stuck segment in our calculation as was explained in section 2, and apply the zero-stress condition on the additional fault segments. Specifically we monitored a fault segment of length 80, where the middle segment of length 50 is treated as a stuck segment with non-zero stress thresholds. We find the same scaling for the size distribution of earthquakes.

In our model, earthquakes with energy greater than $\bar{E}$ typically have ruptures extending, from one side to the other, along the direction of the fault and hence can be viewed as 'great earthquakes'. Though these events are less frequent, they release most of the energy accumulated due to stress build-up. For real earthquakes, however, the size effects have not yet been well established due to limited seismological data on great earthquakes. By using typical numbers (e.g. for the San Andreas fault zone: $v_0 \approx 3.5$ cm/yr, $\mu = 30$ GPa, fault length ≈ 400 km and crust thickness ≈ 50 km), we find that the mean recurrence time of great earthquakes in our model to be of the order of a few hundred years; this is consistent with the recurrence times estimated using seismic moments observed in great earthquakes [2].

We have also studied the distribution for time intervals between successive earthquakes. To understand the size dependence of the temporal correlation, we introduce a lower cut-off, E_l, in the earthquake energy. The time interval is defined for successive earthquakes with energy larger than E_l (i.e. we ignore small earthquakes with energy less than E_l). Figure 5 shows the distributions for various choices of E_l ($\sigma_l = 0.1001$ is used). For $E_l = 0$ (where the statistics is dominated by small earthquakes) the distribution is found to be closer to an exponential, suggesting a Poisson process for the occurrence of small earthquakes; this can be ascribed to the absence of spatial correlations in the thresholds. As E_l increases, a hump around the mean occurrence time for large earthquakes develops

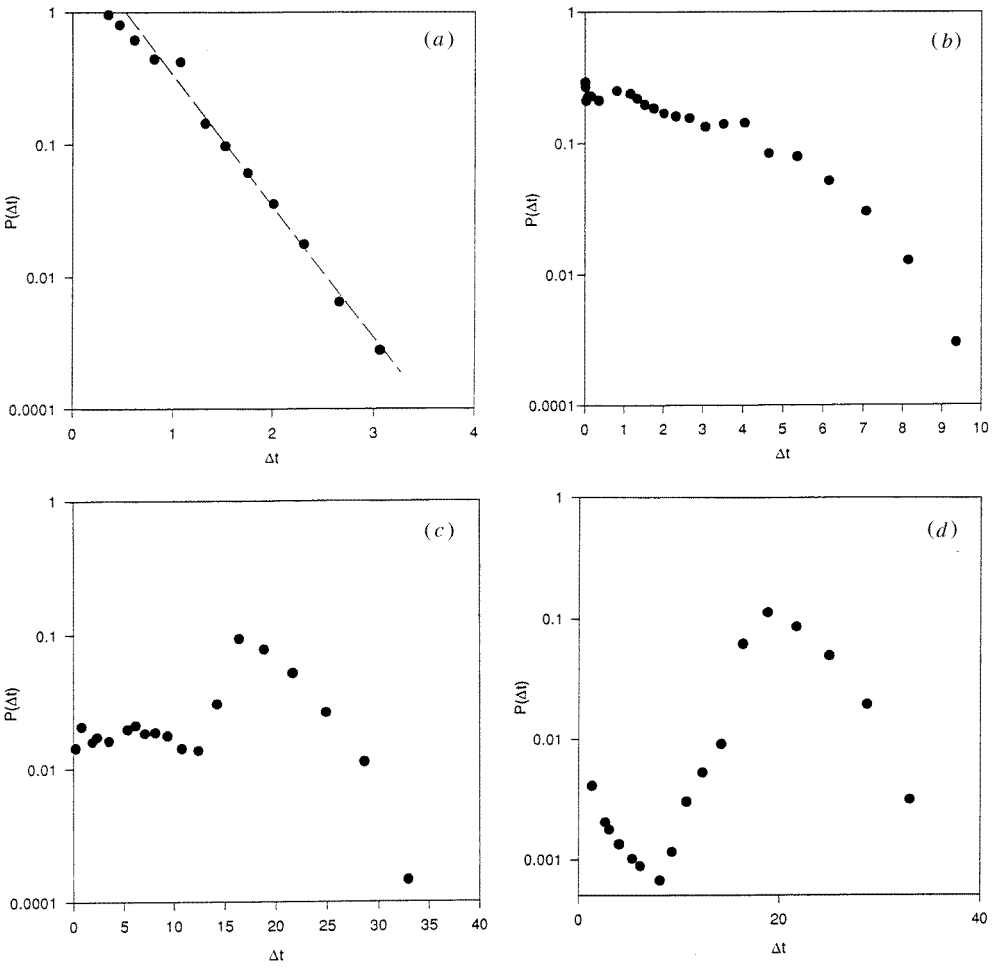

Figure 5. Distribution of time intervals between successive earthquakes with energy released larger than E_l: (*a*) $E_l = 0.0$; (*b*) $E_l = 2.0$; (*c*) $E_l = 50.0$; (*d*) $E_l = 100.0$. Note the exponential distribution in (*a*) and the pronounced hump in (*d*).

in the distribution, suggesting some temporal correlation for large earthquakes. The broad distribution, however, still prevents the prediction of large earthquakes.

5. Conclusions

We have presented a systematic numerical procedure and new techniques for the simulation of quasistatic processes of fractures, and other breakdown problems. The procedure has been applied to a study of a model of a seismic zone with an embedded pre-existing fault structure. We obtain the Gutenberg–Richter law for the model, which is consistent with the seismological data. The scaling laws are found to be very robust; they are insensitive to the degree of spatial inhomogeneities and to whether the model is deterministic or not. The data for the time-interval distribution is consistent with a Poisson process for the occurrence of small earthquakes, but temporal correlations are significant for large earthquakes.

Acknowledgment

We are grateful to the Ohio Supercomputer Center for providing computer time.

Appendix A. Evaluation of the Green functions

In this appendix we discuss how the evaluation of the two-dimensional integrals that occur in the Green functions can be reduced to one-dimensional integrals that can then be handled numerically. Recall that the Green function, $G_\sigma(x, y)$, is given by

$$G_\sigma(x, y) = \int_{-\pi}^{\pi} \frac{\mathrm{d}k_x}{2\pi} \int_{-\pi}^{\pi} \frac{\mathrm{d}k_y}{2\pi} \frac{\sin^2 k_x \sin^2 k_y}{(1 - \cos k_x \cos k_y)^2} \mathrm{e}^{\mathrm{i}k_x x + \mathrm{i}k_y y}.$$

We only need the values of the Green functions for integer values of x and y. For integral x and y, we can first integrate over k_y by doing the complex integral obtained from the change of variable $z = \mathrm{e}^{\mathrm{i}k_y}$:

$$G_\sigma(x, y) = \int_{-\pi}^{\pi} \frac{\mathrm{d}k_x}{2\pi} \sin^2 k_x \mathrm{e}^{\mathrm{i}k_x x} \left[\oint_C \frac{\mathrm{d}z}{2\pi \mathrm{i} z} \frac{\left[\frac{1}{2\mathrm{i}}(z - 1/z)\right]^2 z^y}{\left(1 - \frac{1}{2}\cos k_x (z + 1/z)\right)^2} \right]. \quad \text{(A.1)}$$

The integral in the square bracket can be evaluated as follows:

$$I_1 = -\oint_C \frac{\mathrm{d}z}{2\pi \mathrm{i}} \frac{(z^2 - 1)^2 z^{y-1}}{(2z - \cos k_x z^2 - \cos k_x)^2}. \quad \text{(A.2)}$$

Let us consider the case that $y > 0$. The poles of the integrand can be obtained by solving the equation

$$2z - \cos k_x z^2 - \cos k_x = 0.$$

There are two solutions: $z_{1,2} = (1 \pm |\sin k_x|)/\cos k_x$; only the root $z_1 = (1 - |\sin k_x|)/\cos k_x = \cos k_x/(1 + |\sin k_x|)$ lies inside the unit circle. The integral can be written as

$$I_1 = -\oint_C \frac{\mathrm{d}z}{2\pi \mathrm{i}} \frac{(z^2 - 1)^2 z^{y-1}}{\cos^2 k_x (z - z_1)^2 (z - z_2)^2} = -\frac{\mathrm{d}}{\mathrm{d}z} \left[\frac{(z^2 - 1)^2 z^{y-1}}{\cos^2 k_x (z - z_2)^2} \right]_{z=z_1}$$

or

$$I_1 = -\frac{1}{\cos^2 k_x} \left[\frac{4(z_1^2 - 1) z_1^y}{(z_1 - z_2)^2} + \frac{(y - 1)(z_1^2 - 1)^2 z_1^{y-2}}{(z_1 - z_2)^2} - \frac{2(z_1^2 - 1)^2 z_1^{y-1}}{(z_1 - z_2)^3} \right].$$

Using the fact that $z_1 z_2 = 1$, we can further simplify the expression

$$I_1 = \frac{1}{\cos^2 k_x} \left[\frac{2z_1^{y+2}}{1 - z_1^2} - (y - 1) z_1^y \right] = \frac{z_1^y}{\sin^2 k_x + |\sin k_x|} - (y - 1) \frac{z_1^{y-2}}{(1 + |\sin k_x|)^2}. \quad \text{(A.3)}$$

Now we have reduced the two-dimensional integral to a one-dimensional integral. For the case that $y = 0$, we can show, by adding the contribution from the pole $z = 0$, that

$$I_1 = \frac{1}{\cos^2 k_x} \left[\frac{2z_1^2}{1 - z_1^2} \right] = \frac{1}{\sin^2 k_x + |\sin k_x|}. \quad \text{(A.4)}$$

Thus for $y \geqslant 0$ the Green function can be written as

$$G_\sigma(x, y) = \int_0^{\pi} \frac{\mathrm{d}k_x}{\pi} |\sin k_x| \cos k_x x \left[\frac{z_1^y}{1 + |\sin k_x|} - \eta(y) \frac{|\sin k_x| y_1^{y-2}}{(1 + |\sin k_x|)^2} \right] \quad \text{(A.5)}$$

where $\eta(y) = y - 1$ if $y > 1$ and $\eta(y) = 0$ when $y = 0, 1$.

Appendix B. Details of the numerical matrix inversion scheme

We are interested in solving an equation of the form

$$\sum_j A_{ij} f_j = b_i \tag{B.1}$$

where A is an $N \times N$ matrix with N being the number of double couples, and the matrix elements of A are the values of the appropriate Green functions. The vector, f, contains the double-couple strengths, which we want to obtain from the equations. The vector, b, depends on the external boundary conditions and the boundary conditions imposed at the ruptured sites as described in section 3. For example, let i_0 denote the position of a newly ruptured site; let us impose the boundary condition that the stress at the site is reduced to zero after the rupture, the external boundary condition remaining unchanged. Then the matrix element $A_{i_0 j}$ is given by $G_\sigma(\boldsymbol{r}_{i_0} - \boldsymbol{r}_j)$ and b_{i_0} is given by $-\sigma^{\text{old}}(\boldsymbol{r}_{i_0})$ ($\sigma^{\text{old}}(\boldsymbol{r}_{i_0})$ is the stress at i_0 just before the rupture) so that the new stress is fixed to zero. If, on the other hand, i_0 is a site on a stuck segment of the fault, then $A_{i_0 j}$ will be related to the Green functions for the displacement: $A_{i_0 j} = G_u(\boldsymbol{r}_{i_0} + \hat{e}_y/2 - \boldsymbol{r}_j) - G_u(\boldsymbol{r}_{i_0} - \hat{e}_y/2 - \boldsymbol{r}_j)$ and the corresponding b_{i_0} is zero (if there are no changes in the external boundary conditions).

The idea is to keep a copy of the current matrix B which is the inverse of A. The matrix B is updated at each step, and the solution for the double-couple strengths is obtained using $f = Bb$. We consider here the updating of B due to one new rupture (it can be generalized easily to the case of many new ruptures). Typically there are two types of new ruptures: (a) a completely new rupture at a previously elastic site and (b) a new rupture at a pre-existing ruptured site (the boundary condition at the ruptured site is changed from being a stuck ruptured interface to a slipping interface with a stress reduction). For case (a), the matrix A can be partitioned as

$$A = \begin{bmatrix} A_{\text{old}} & A_1 \\ A_2 & A_3 \end{bmatrix} \tag{B.2}$$

where A^{old} is the matrix A before the rupture, A_1 is a column vector, A_2 is a row vector, and A_3 is a scalar. Let $\boldsymbol{r}_i, i = 1, 2, \ldots, N$ be the locations of previous ruptures (N is the total number of ruptures before the current one) and $\boldsymbol{r}_{N+1}$ be the location of the current rupture. Then $A_1[i] (i = 1, 2, \ldots, N)$ are given by

$$A_1[i] = G_\sigma(\boldsymbol{r}_i - \boldsymbol{r}_{N+1})$$

if constant stress boundary condition is employed at r_i, and

$$A_1[i] = G_u\left(\boldsymbol{r}_i - \boldsymbol{r}_{N+1} + \frac{\hat{e}_y}{2}\right) - G_u\left(\boldsymbol{r}_i - \boldsymbol{r}_{N+1} - \frac{\hat{e}_y}{2}\right)$$

if stuck boundary condition is employed at $\boldsymbol{r}_i$. A_2 and A_3 are simply given by

$$A_2[i] = G_\sigma(\boldsymbol{r}_{N+1} - \boldsymbol{r}_i) \qquad i = 1, \ldots, N \text{ and } A_3 = G_\sigma(0, 0).$$

The new matrix B, which is the inverse of the new matrix A, is given by the following formulae [5]:

$$B = A^{-1} = \begin{bmatrix} B_0 & B_1 \\ B_2 & B_3 \end{bmatrix} \tag{B.3}$$

where $B_3 = (A_3 - A_2 B_{\text{old}} A_1)^{-1}$, $B_0 = B_{\text{old}} + (B_{\text{old}} A_1) B_3 (A_2 B_{\text{old}})$, $B_1 = -(B_{\text{old}} A_1) B_3$, and $B_2 = -B_3(A_2 B_{\text{old}})$. It is easy to see that, given $B_{\text{old}} = A_{\text{old}}^{-1}$, one can obtain the new matrix B with a calculation of order of N^2.

For case (b), the size of the matrix is unaltered, but one row of the matrix has changed. Let the index of the row whose elements are changed (corresponding to a previously ruptured site rupturing again) be i_0; then the new matrix A can be decomposed as

$$A = A_{\text{old}} + u \bigotimes v$$

where u is a vector with unity at element i_0 and zero everywhere else, v is the vector containing the difference between the i_0th row of A and A_{old}. For our case,

$$v[i] = G_\sigma(\boldsymbol{r}_{i_0} - \boldsymbol{r}_i) - \left[G_u\left(\boldsymbol{r}_{i_0} - \boldsymbol{r}_i + \frac{\hat{e}_y}{2}\right) - G_u\left(\boldsymbol{r}_{i_0} - \boldsymbol{r}_i - \frac{\hat{e}_y}{2}\right)\right] \qquad i = 1, \ldots, N. \tag{B.4}$$

With A expressed in this form, we can use the Sherman–Morrison formulae [5] to obtain the inverse of A:

$$B = A^{-1} = B_{\text{old}} - \frac{(B_{\text{old}}u) \otimes (vB_{\text{old}})}{1 + vB_{\text{old}}u}. \tag{B.5}$$

It is easy to check that, given $B_{\text{old}} = A_{\text{old}}^{-1}$, this also requires a calculation of order N^2 to obtain the new matrix B.

References

[1] Herrmann H J and Roux S 1990 *Statistical Models for the Fracture of Disordered Media* (Amsterdam: North Holland)
[2] Knopoff L 1990 *Disorder and Fracture* ed C Charmet *et al* (New York: Plenum) p 279
[3] Xu H J, Bergersen B and Chen K 1992 *J. Phys. A: Math. Gen.* **25** L1251
Xu H J, Bergersen B and Chen K 1993 *J. Physique I* **3** 2029
[4] Aki K and Richards P G 1980 *Quantitative Seismology, Theory and Methods* (San Francisco, CA: Freeman)
[5] Press W H, Teukolsky S A, Vetterling W T and Flannery B P 1992 *Numerical Recipes–The Art of Scientific Computing* 2nd edn (Cambridge: Cambridge University Press)
[6] de Arcangelis L, Redner S and Herrmann H J 1985 *J. Physique Lett.* **46** L585
[7] Duxbury P M, Leath P L and Beale P D 1987 *Phys. Rev.* B **36** 367
[8] Bhagavatula R, Chen K, Jayaprakash C and Xu H J 1994 *Phys. Rev.* E **49** 5001–6
[9] Niemeyer L, Pietronero L and Wiesmann H J 1984 *Phys. Rev. Lett.* **52** 1033
[10] Bhagavatula R, Chen K and Jayaprakash C 1994 *J. Phys. A: Math. Gen.* **27** L155–62
[11] Bhagavatula R, Chen K and Jayaprakash C 1995 *Geophys. Res. Lett.* **22** 1301
[12] Scholz C H 1990 *The Mechanics of Earthquakes and Faulting* (Cambridge: Cambridge University Press)
[13] Grinstein G 1995 *Scale Invariance, Interfaces and Non-equilibrium Dynamics* ed A McKane, M Droz, J Vannimenus and D Wolf (New York: Plenum)
[14] Burridge R and Knopoff L 1967 *Bull. Seismol. Soc. Am.* **57** 341
[15] Takayasu H and Matsuzaki M 1988 *Phys. Lett.* A **131** 244
[16] Sornette A and Sornette D 1989 *Europhys. Lett.* **9** 192
Miltenberger P, Sornette D and Vanneste C 1993 *Phys. Rev. Lett.* **71** 3604 and references therein
[17] Brown S R, Scholz C H and Rundle J B 1991 *Geophys. Res. Lett.* **18** 215
[18] Ito K and Matsuzaki M 1990 *J. Geophys. Res.* **95** 6853
[19] Nakanishi H 1990 *Phys. Rev.* A **41** 7086–9
[20] Olami Z, Feder H S and Christensen K 1991 *Phys. Rev. Lett.* **68** 1244
[21] Bak P and Chen K 1995 *Fractals in the Earth Sciences* ed C Barton and P LaPointe (Denver, CO: Geological Society of America) and references therein
[22] Bak P, Tang C and Wiesenfeld K 1987 *Phys. Rev. Lett.* **59** 381
[23] Gutenberg B and Richter C F 1956 *Ann. di Geofis.* **9** 1
[24] Carlson J M and Langer J S 1989 *Phys. Rev. Lett.* **62** 2632
Carlson J M and Langer J S 1989 *Phys. Rev.* A **40** 2803
[25] Carlson J M 1991 *Phys. Rev.* A **44** 6226
[26] Shaw B E, Carlson J M and Langer J S 1992 *J. Geophys. Res.* **97** 479
[27] Shaw B E 1995 *J. Geophys. Res.* **100** 18239

[28] Knopoff L, Landoni J A and Abinante M S 1992 *Phys. Rev.* A **46** 7445
[29] Lomnitz-Adler J 1993 *J. Geophys. Res.* **98** 17745
[30] Ben-Zion Y and Rice J R 1993 *J. Geophys. Res.* **98** 14109
[31] Chen K, Bak P and Obukhov S P 1991 *Phys. Rev.* A **43** 625
[32] Scholz C H and Mandelbrot B B (eds) 1989 *Fractals in Geophysics* (Basel: Birkhäuser)
[33] Reid H F 1910 *The California Earthquake of April 18, 1906* Carnegie Institute of Washington, Publ no 87 vol 2
[34] Pacheco J F, Scholz C H and Sykes L R 1992 Changes in frequency-size relationship from small to large earthquakes *Nature* **355** 71–3